Science of the Total Environment 883 (2023) 163733

Contents lists available at ScienceDirect

Science of the Total Environment

journal homepage: www.elsevier.com/locate/scitotenv

Atmospheric ammonia in China: Long-term spatiotemporal variation, urban-rural gradient, and influencing factors

Jinyan Dong [a], Baojie Li [a,*], Yan Li [a], Rui Zhou [b], Cong Gan [a], Yongqi Zhao [a], Rui Liu [a], Yating Yang [a], Teng Wang [c], Hong Liao [a]

[a] *Collaborative Innovation Center of Atmospheric Environment and Equipment Technology, Jiangsu Key Laboratory of Atmospheric Environment Monitoring and Pollution Control, School of Environmental Science and Engineering, Nanjing University of Information Science & Technology, Nanjing 210044, China*

[b] *College of Resources and Environment, University of Chinese Academy of Sciences, Beijing, China*

[c] *College of Oceanography, Hohai University, Nanjing 210098, China*

HIGHLIGHTS

- The vertical column densities (VCDs) of NH_3 in China have increased significantly (by 31.88%) from 2008 to 2019.
- Significant variations in NH_3 VCDs were observed between urban and rural areas in China.
- The overall urban-rural gap temporal behavior of NH_3 VCDs in China showed a widening trend.
- The decreased acid gas concentration contributed to the increase in NH_3 VCDs using GTWR model.

GRAPHICAL ABSTRACT

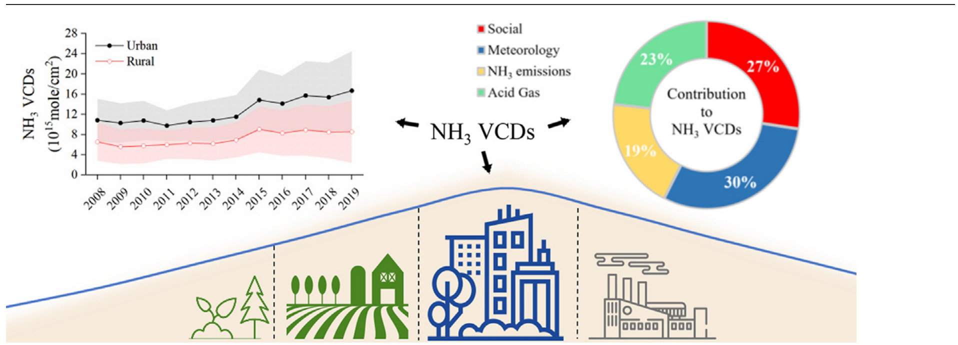

ARTICLE INFO

Editor: Philip K. Hopke

Keywords:
Atmospheric ammonia
IASI
Spatiotemporal distribution
Urban-rural gradient
GTWR

ABSTRACT

In recent years, atmospheric ammonia (NH_3) concentrations have increased in China. Ammonia control has become one of the next hot topics in air pollution mitigation with the increasing cost of acid gas emission reduction. In this study, using Infrared Atmospheric Sounding Interferometer (IASI) satellite observations, we analyzed the spatiotemporal distribution, the urban-rural gradient of the vertical column densities (VCDs) of NH_3 and the contribution of influencing factors (meteorology, social, atmospheric acid gases, and NH_3 emissions) in China from 2008 to 2019 using hotspot analysis, circular gradient analysis, geographical and temporal weighted regression, and some other methods. Our results showed that NH_3 VCDs in China have significantly increased (31.88 %) from 2008 to 2019, with the highest occurring in North China Plain. The average NH_3 VCDs in urban areas were significantly higher than those in rural areas, and the urban-rural gap in NH_3 VCDs was widening. The results of circular gradient analysis showed an overall decreasing trend in NH_3 VCDs along the urban-rural gradient. We used a geographically and temporally weighted regression model to analyze the contribution of various influencing factors to NH_3 VCDs: meteorology (30.13 %), social (27.40 %), atmospheric acid gases (23.20 %), and NH_3 emissions (19.28 %) factors. The results showed substantial spatiotemporal differences in the influencing factors. Atmospheric acid gas was the main reason for the increase in NH_3 VCDs from 2008 to 2019. A more thorough understanding of the spatiotemporal distribution, urban-rural variations, and factors influencing NH_3 in China will aid in developing control strategies to reduce $PM_{2.5}$.

1. Introduction

Atmospheric ammonia (NH_3) is the main alkaline gas in the atmosphere and plays an important role in atmospheric chemistry. NH_3 reacts with

* Corresponding author.
E-mail address: baojieli@nuist.edu.cn (B. Li).

http://dx.doi.org/10.1016/j.scitotenv.2023.163733
Received 5 January 2023; Received in revised form 16 March 2023; Accepted 21 April 2023
Available online 26 April 2023

acidic gases (e.g., SO_2 and NO_X) rapidly to form ammonium salts, which have negative effects on air quality, human health, and climate change (Sharma et al., 2014; Xu et al., 2019a; Zhang et al., 2017). Since the 1980s, China has become a major region for global NH_3 emissions (Streets et al., 2003) due to a substantial increase in intense human activities such as fertilization and livestock production (Fowler et al., 2013; Kang et al., 2016; Liao et al., 2022). It is known that NH_3 is an important contributor to the $PM_{2.5}$ (particulate matter ≤ 2.5 μm in aerodynamic diameter) component, especially in smoggy weather (Qiao et al., 2018). It has been reported that agricultural NH_3 emissions alone contribute to 30 % of $PM_{2.5}$ formation in the North China Plain (An et al., 2019).

It has been reported that controlling NH_3 emissions can greatly improve air quality (Xu et al., 2019a, 2017). However, China has very few policies on the management and control of NH_3 emissions. Since 2011, the strong control of air pollution in China has reduced atmospheric concentrations of sulfur dioxide (SO_2) and nitrogen oxides (NO_X) successfully, which has greatly influenced the concentration of NH_3 (Liu et al., 2017a). The cost of reducing emissions of other major air pollutants increases and controlling NH_3 emissions becomes more important. Long-term NH_3 observation analysis is important for the environmental burden of NH_3 emissions and control strategies (Liu et al., 2017a, 2017b; Xu et al., 2018).

Satellite observations are superior to ground-based observations in terms of resolution and range. The most accurate way to measure NH_3 in the atmosphere is through ground-based instrument monitoring (Wu et al., 2018; Xu et al., 2019b). However, there are few long-term observations in China, only the National Nitrogen Deposition Monitoring Network (NNDMN) (Xu et al., 2015b) and the Ammonia Monitoring Network (AMoN-China) (Pan et al., 2018b). Long-term environmental monitoring of NH_3 by ground-based instruments remains a major challenge. Compared with in situ observations, satellite observations based on advanced infrared spectroscopy (IR) detectors (e.g., Infrared Atmospheric Sounding Interferometer (IASI), Tropospheric Emission Spectrometer (TES), Cross-Orbit Infrared Sounder (CrIS), etc.) can obtain long-term, high-spatial-resolution NH_3 columns. Satellite observations of NH_3 have been widely used for spatio-temporal analysis at global and national scales (Liu et al., 2017b; Shephard and Cady-Pereira, 2015; Van Damme et al., 2014; Warner et al., 2016; Zhang et al., 2017), as well as for impact factor analysis (Deng et al., 2021; He et al., 2021; Hickman et al., 2021).

No consensus has been reached on whether the main source of urban NH_3 is agricultural or nonagricultural so far (Gu et al., 2022; Pan et al., 2018a). Because of its short lifetime, NH_3 may be difficult to transport over long distances from its source (Möller and Schieferdecker, 1985). The main source of ammonia in the urban atmosphere is likely local rather than long-distance transport (Gu et al., 2022; Liao et al., 2022). The study found that non-agricultural sources account for 71 % of Beijing's total ammonia emissions (Gu et al., 2022). According to other studies, NH_3 emissions from agriculture are an increasingly important precursor of particulate $PM_{2.5}$ pollution in urban environments. A vertical isotopic study on a 325 m meteorological tower in urban Beijing showed that fertilizer volatilization contributed 40 % to the total NH_3 at 320 m, which was three times that at 2 m (Zhang et al., 2020). It has been reported that agricultural sources contributed 84 % to the total atmospheric ammonia during the clean days in urban Beijing (Pan et al., 2016). Meteorological conditions, such as wind speed and direction, can affect the composition of urban ammonia sources by influencing pollutant dispersion and atmospheric transport (Pan et al., 2016; Zhang et al., 2020). The differences in the composition of urban ammonia sources may be influenced by weather conditions and agricultural activities (Lan et al., 2021; Pan et al., 2016; Zhang et al., 2020).

Currently, few studies have examined urban-rural differences in NH_3 vertical column densities (VCDs) at the national scale, and the spatial variation and temporal trends of NH_3 in urban and rural China are not clear. Furthermore, few studies have analyzed the influences of NH_3 VCDs on a national scale in multiple aspects, including meteorology, social, atmospheric acid gases, and NH_3 emissions. Some studies have only analyzed the effect of acid gases on NH_3 VCDs in North China (Deng et al., 2021), or the effect of emissions on NH_3 (Fu et al., 2015), etc. A more thorough understanding of the spatiotemporal distribution, urban-rural variations, and factors influencing NH_3 in China will aid in developing control strategies to reduce $PM_{2.5}$.

In this study, we used long-term IASI satellite observations to analyze the characteristics of the spatial and temporal variations of NH_3 VCDs in China from 2008 to 2019. We analyzed the urban-rural variation in NH_3 VCDs and investigated the patterns and temporal trends in urban-rural gradients using circular buffer analysis. We also analyzed the contribution of various influencing factors (meteorological parameters, atmospheric acid gases, NH_3 emissions, and social factors) to these spatiotemporal variations in NH_3 VCDs using the geographically and temporally weighted regression (GTWR) method.

2. Materials and methods

2.1. Data sources

The reanalyzed IASI-NH_3 dataset is available from the Infrared Atmospheric Sounding Interferometer (IASI) on board MetOp-A (https://iasi.aeris-data.fr/nh3_iasi_a_arch/) (Franco et al., 2018; Van Damme et al., 2017; Whitburn et al., 2016). Our analysis covered the period from January 1, 2008, to December 31, 2019. Some studies suggest that observations from the morning (09:30 a.m.) are generally more sensitive to NH_3 because of the higher thermal contrast at this time of day (Clarisse et al., 2009; Van Damme et al., 2014). Therefore, only daytime (09:30) satellite observations were used for this study. The NH_3 emission data were acquired from the Multiresolution Emission Inventory for China website (MEIC: http://www.meicmodel.org) (Li et al., 2017; Zheng et al., 2018). The undisclosed data of MEIC for 2018 was replaced with data from 2017. The NO_2 columns are available from the NASA Ozone Monitoring Instrument (OMI) standard nitrogen dioxide (NO_2) product (SPv3), which is publicly available from NASA's Goddard Earth Science (GES) Data and Information Service (DISC) (https://disc.gsfc.nasa.gov/uui/datasets/OMNO2_V003/summary). The SO_2 columns are available from the OMI PCA SO_2 product, which is publicly available from NASA's Goddard Earth Sciences (GES) Data and Information Services Center (DISC) (http://disc.sci.gsfc.nasa.gov/Aura/data-holdings/OMI/OMSO2_v003.shtml). The meteorological data are available from the ERA5-Land monthly averaged data (https://cds.climate.copernicus.eu/cdsapp#!/dataset/reanalysis-era5-land-monthly-means?tab=overview) of the European Centre for Medium-Range Weather Prediction (ECMWF), including data on monthly precipitation, 2 m temperature, and 10 m wind speed. Population density data are available from Landscan Global Population Distribution Data (https://landscan.ornl.gov/landscan-datasets). The annual urban extents dataset at 1 km resolution was obtained from (https://doi.org/10.6084/m9.figshare.9828827.v5) (Zhao et al., 2022). The land cover type data used the Landsat-derived annual China Land Cover Dataset (CLCD) (Yang and Huang, 2021). We calculated the area ratio of impervious surface area (hereafter referred to as ISAR) for each raster at the spatial resolution of 10 km.

2.2. Methods

2.2.1. Spatiotemporal analysis of NH_3 VCDs

We constructed a month-by-month IASI NH_3 series and filtered data with cloud coverage above 25 % (Van Damme et al., 2015). We used kriging interpolation to obtain the spatial distribution of monthly NH_3 VCDs by NH_3 monthly series data with a spatial resolution of 5 × 5 min (roughly 10 × 10 km) (Sampson et al., 2013). The annual average NH_3 VCDs was obtained by arithmetic averaging of monthly data. We have performed quality control on the data (Fig. S7). The cross-validation results have shown good correlation (average 0.66). We found that the kriging interpolation performed best in summer. Research has shown, given the strong dependence on thermal contrast, that spring-summer months are better suited to accurately measure NH_3 from IASI (Van Damme et al., 2014). Due to the limited amount of satellite data, using the error-weighted average to obtain NH_3 VCDs can't obtain nationwide data. But we have compared the spatial distribution of NH_3 VCDs obtained by error-weighted averaging (columns with an associated relative above 100 % and cloud coverage above 25 % have been filtered). Our results are highly correlated with the NH_3 data obtained by error-weighted averaging in the grid with values (Fig. S8). The spatial distribution of NH_3 is also basically the same for both methods (Fig. S9).

The hot spot analysis can identify hot and cold spots of NH_3 VCDs with different levels of saliency and we use it to analyze spatial clustering characteristics. We used the Gettis-Ord Gi* statistic to identify the tendency for positive spatial clustering and the location of pockets of high and low spatial association (Getis and Ord, 2010).

The Mann-Kendall test was used to test the significance of the NH_3 VCDs trend in the present study (Mann, 1945; Kendall, 1975). Trend analysis is a linear regression analysis of variables to discover their tendency and degree of change over time. We used the least squares method to fit a one-dimensional linear regression equation to study the time trend and degree of change of NH_3 VCDs on the raster scale, and the formula is as follows:

$$Slope = \frac{n \sum_{i=1}^{n} (i \times x_i) - \sum_{i=1}^{n} x_i \sum_{i=1}^{n} i}{n \sum_{i=1}^{n} i^2 - \left(\sum_{i=1}^{n} i\right)^2} \tag{1}$$

where *slope* represents the trend of NH_3 VCDs for each image element, n is the number of years and x_i represents the average NH_3 VCDs in year i.

2.2.2. Urban-rural gradient analysis

We further studied the urban-rural gradients in the 31 provincial capitals. We resampled the spatial resolution of the NH_3 VCDs to 1 km to fit the annual urban extents dataset. We established five circular buffers of 10, 20, 30, 40, and 50 km around the urban area of the provincial capital city and obtained the average NH_3 VCDs of the core urban areas over the 12 years in the sample cities through circular buffer division. For example, a 50 km buffer zone is indicated as a circular area between 40 km and 50 km from the current year's city limits. The average NH_3 VCDs in the circular buffer zone exclude data from urban areas to reduce errors.

Due to the differences in NH_3 VCDs levels among provincial capitals, the urban-rural gradients were analyzed by the ratio of average NH_3 VCDs in the circular buffer zones to urban areas, and the formula is expressed as:

$$D_s^{i,t} = \frac{\mu_s^{i,t}}{\mu_0^{i,t}} \tag{2}$$

where
D_s^i is the ratio of annual NH_3 VCDs in the buffer zone to the urban area in city i, μ_s^i is the average NH_3 VCDs in the s km ($s = 0$ km (urban areas), 10 km, 20 km, …, 50 km) buffer zone in city i, and μ_0 is the average NH_3 VCDs in the urban area.

Through buffer analysis, we extracted two types of cities based on the urban-rural gradient characteristics of NH_3 VCDs: (1) cities with substantially larger densities than those in surrounding areas were considered NH_3 hot spot cities ($D_{30} < 90$ %, hereafter referred to as hot spot cities); (2) cities with lower densities than the surrounding areas were considered NH_3 cold spot cities ($D_{30} > 100$ %, hereafter referred to as cold spot cities).

2.2.3. Quantitative analysis of influencing factors

Previous studies have shown that the possible reasons behind the observed long-term trends include changes in NH_3 emissions, anthropogenic SO_2 and NOx emissions, ammonia phase partitioning, and meteorology (Yu et al., 2018). Urban impervious surfaces are an important feature of urban areas, and urban impervious areas in China have been expanding rapidly in recent years (Yang and Huang, 2021). The impervious surface areas reflect the level of urban development (Kuang et al., 2014). We have found that NH_3 VCDs exists at high concentrations over impervious surfaces. In this study, we used the IASR to refer to the level of urbanization. Based on these studies, we quantified the contribution of influential factors to NH_3 VCDs at city-level from four aspects: NH_3 emissions, atmospheric acid gases (SO_2 and NO_2), meteorological parameters (temperature, wind speed, and precipitation), and social factors (population density and ISAR).

The geographically and temporally weighted regression (GTWR) is an extension of a traditional regression model, the GTWR model can simultaneously consider both spatial and temporal heteroscedasticity and thus provide spatiotemporal estimations (Chu et al., 2015; Huang et al., 2010; Wang et al., 2012; Wu et al., 2014). The GTWR model can be described as:

$$Y_i = \beta_0(\mu_i, \upsilon_i, t_i) + \sum_k \beta_k(\mu_i, \upsilon_i, t_i) X_{i,K} + \varepsilon_i \tag{3}$$

where Y_i is the dependent variable of the ith sample (i.e., normalized of the city mean of NH_3 VCDs in this study), $X_{i,k}$ are the independent variables of the ith sample (i.e., normalized of the city mean of climate variables, NH_3 emissions and other influencing factors in this study), μ_i, ν_i, and t_i are the space-time coordinates of sample i, and $\beta_k(\mu_i, \nu_i, t_i)$ is the estimated coefficient of independent variable k for sample i. The weighted least squares (WLS) approach was adopted to calibrate GTWR (Huang et al., 2010). All independent and dependent variables were calculated as city means and standardized with the *Z*-SCORE model before running the GTWR.

The regression coefficients of 367 cities in 12 years were obtained by GTWR. We obtain the contribution rate of each city's impact factor through the regression coefficients, and the formula can be expressed as:

$$C_{i,j}^t = \frac{\left|\lambda_{i,j}^t \times x_{i,j}^t\right|}{\sum_{j=1}^{k} \left|\lambda_{i,j}^t \times x_{i,j}^t\right|} \tag{4}$$

where $C_{i,j}$ is the annual contribution rate of the jth influencing factor in city i, $\lambda_{i,j}$ is the regression coefficient of the influencing factors j in city i, and $x_{i,j}$ are the independent variables of the city i (i.e., normalized of the city mean of climate variables, NH_3 emissions and other influencing factors in this study), k is the number of elements (i.e., 8 elements). The contribution rate of the influencing factors of the four categories was obtained by adding the contribution rate of each element of the category.

3. Results

3.1. Spatio-temporal characteristics of NH_3 VCDs

3.1.1. Annual variation of NH_3 VCDs

The average NH_3 VCDs in China was 7.28×10^{15} molec·cm^{-2} from 2008 to 2019. The annual average NH_3 VCDs showed a significant upward trend (tau = 0.64, $p < 0.01$) (Table S1), with an average annual growth rate of 1.85 % from 2008 (7.39×10^{15} molec·cm^{-2}) to 2019 (8.67×10^{15} molec·cm^{-2}) (Fig. 1a). NH_3 VCDs peaked in 2015 (9.09×10^{15} molec·cm^{-2}), being 1.61 times higher than the lowest value, which was recorded in 2009 (5.64×10^{15} molec·cm^{-2}). The trend in NH_3 VCDs was relatively stable from 2008 to 2014. We noted a substantial increase between 2014 (6.99×10^{15} molec·cm^{-2}) and 2015 (9.09×10^{15} molec·cm^{-2}), which was an increase of 30 %. This could have been caused by a decrease in the concentration of acid gases in the atmosphere and the nonlinear response of acid gases in the atmosphere to NH_3, which we discuss in detail in Section 3.3. NH_3 VCDs decreased slightly from 2015 (9.09×10^{15} molec·cm^{-2}) to 2019 (8.67×10^{15} molec·cm^{-2}). This was probably caused by the reduction of NH_3 emissions (Liao et al., 2022). The average annual growth rate of NH_3 VCDs in Central China (CC) is 5.80 %, which is 2.8 times the national average annual growth rate and the highest among all regions. Except for northern Xinjiang and Tibet, NH_3 VCDs showed an increasing trend in most regions of China (Fig. 2), and the average change rate in China was 0.32×10^{15} molec·cm^{-2}·yr^{-1}. The fastest-growing regions were concentrated in the North China Plain (NCP) as well as the Sichuan Basin, with an average change rate of 1.0×10^{15} molec·cm^{-2}·yr^{-1} in NCP. These regions, characterized by dense population and developed agriculture, exhibit high levels of NH3 emissions in China. Research has

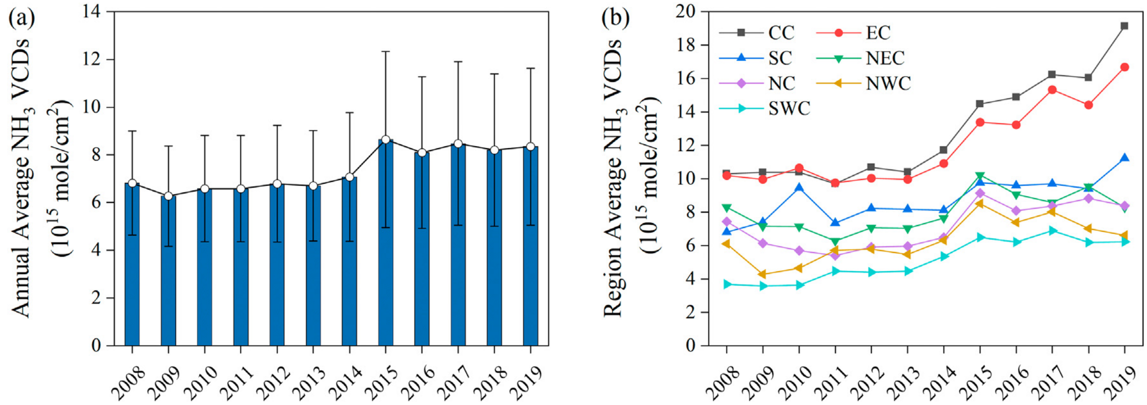

Fig. 1. Long-term trends in annual average NH_3 VCDs from 2008 to 2019. (a) Interannual variation of annual average NH_3 VCDs in China and (b) interannual variation of annual average NH_3 VCDs in different geographic regions, including central China (CC), east China (EC), north China (NC), northeast China (NEC), south China (SC), southwest China (SWC) and northwest China (NWC).

found that sulfur dioxide (SO_2) emissions sharply decreased by about 60 % between 2008 and 2016 (Liu et al., 2018). This significant reduction in SO_2 emissions is the main driver of the rapid increase in ammonia concentrations observed in these areas (Liu et al., 2018).

3.1.2. Spatial distribution characteristics of NH_3 VCDs

Owing to the differences in natural resources, social development goals, and economic and industrial structures in different regions of China, we found remarkable regional differences in the spatial distribution of NH_3 VCDs (Fig. 3). The results of hotspot analysis indicated that spatial distribution of NH_3 VCDs in China was strongly clustered (Fig. 2b). The high concentrations mainly appeared the North China Plain region, Sichuan Basin and northern Xinjiang, while the low concentrations mainly appeared over the Qinghai-Tibet regions, northern Inner Mongolia and central Xinjiang. The trend analysis results reflected the spatial distribution of the annual variation trend of NH_3 VCDs (Fig. 2a). Regions with faster annual change rate (Slope > 1.0×10^{15} molec·cm^{-2}·yr^{-1}) were concentrated in the North China Plain. Owing to the high correlation between NH_3 emissions and human activities and intensive agricultural activities, the spatial distribution of NH_3 VCDs showed high consistency with population density and cultivated land. NH_3 VCDs peaked in CC (average 12.86×10^{15} molec·cm^{-2}), which was 1.77 times the national average. The average NH_3 VCDs in other regions were EC (average 12.05×10^{15} molec·cm^{-2}), SC (average 8.77×10^{15} molec·cm^{-2}), NEC (average 8.03×10^{15} molec·cm^{-2}), NC (average 7.15×10^{15} molec·cm^{-2}), NWC (average 6.32×10^{15} molec·cm^{-2}), and SWC (average 5.13×10^{15} molec·cm^{-2}), respectively. Shandong Province was the highest (18.47×10^{15} molec·cm^{-2}) at provincial region levels. In summary, the distribution of NH_3 VCDs in China was high concentrations in the east and low concentrations in the west, with the highest concentrations in North China Plain. High concentrations were distributed around human and cropland activities. NH_3 VCDs were characterized by regional aggregation, which was caused by the intensification of production, agricultural activities, and animal husbandry in China.

3.1.3. Differences in NH_3 VCDs over different land covers

Based on the land cover type data, we obtained the average NH_3 VCDs for the different land cover types during 2008–2019 (Fig. 4). NH_3 VCDs over different surface cover types showed an increasing trend, with the most significant increase in cropland (tau = 0.73, $p < 0.01$) (Table S1). We found that the average NH_3 VCDs over impervious surfaces were substantially higher than those of the other types, by 1.95 times on average, and their average annual growth rate was also high (4.26 %), being 1.67 times higher than the average. The impervious surface is the most important feature of human settlements and a key indicator of urbanization (Gong et al., 2019). Urban NH_3 emissions are mainly from municipal waste and fossil fuel combustion (road traffic, industrial emissions, domestic coal, etc.) (Chen et al., 2020; Reche et al., 2015; Sun et al., 2017). NH_3

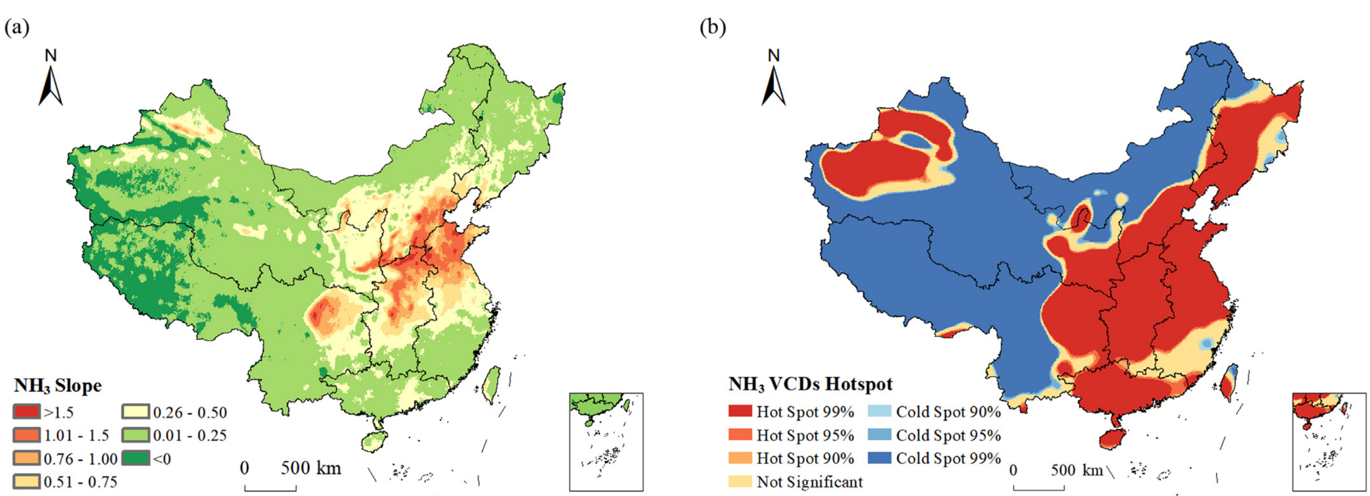

Fig. 2. Spatio-temporal characteristics of NH_3 VCDs. (a) Spatial distribution of NH_3 VCDs interannual variability in China and (b) the hotspot analysis of average NH_3 VCDs in China from 2008 to 2019.

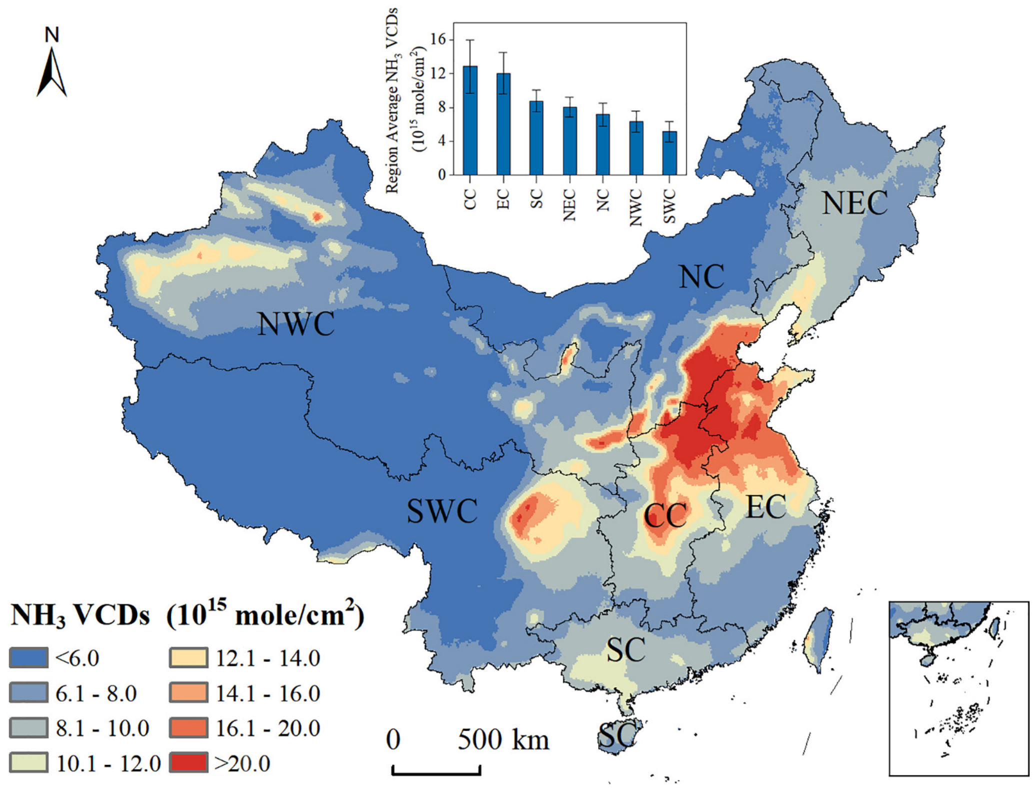

Fig. 3. Spatial distribution of average NH_3 VCDs in China from 2008 to 2019.

emission source intensity is high in urban areas due to urbanization and the resulting population concentration (Liao et al., 2022; Reche et al., 2015). It has been reported that about 12 % of the land area contributed to >70 % of the emissions in 2017 (Ma, 2020).

We also analyzed the temporal variation of NH_3 VCDs over different land cover types (Fig. 4b). The average concentration and average annual growth rate of NH_3 VCDs above cropland cover were 11.20×10^{15} molec·cm^{-2} and 3.72 %, respectively. Farmland is the main area of agricultural production activities, and long-term input of a large amount of fertilizer leads to high near-surface NH_3 emissions in a farmland area. The average value and average annual growth rate of NH_3 VCDs above forest cover were 7.62×10^{15} molec·cm^{-2} and 3.25 %, respectively. The average concentration of NH_3 VCDs over the bare cover was 5.86×10^{15} molec·cm^{-2}. The average NH_3 VCDs for the other land cover types was 5.01×10^{15} molec·cm^{-2}.

3.1.4. Seasonal variations of NH_3 VCDs

The temporal distribution of NH_3 VCDs has obvious seasonal characteristics. NH_3 VCDs was highest in summer and lowest in autumn and winter (Fig. 5). Based on the spatial NH_3 VCDs distribution throughout the seasons (Fig. S1), we found that NH_3 VCDs in the North China Plain was significantly higher during summer. These phenomena were closely related to the seasonal characteristics of agricultural emissions and the seasonal variations in meteorological conditions (Dai et al., 2019; Li et al., 2021; Liu et al., 2017b). It has been reported that >40 % of fertilizer applications and >25 % of livestock emissions occur in the summer (Kang et al., 2016; Xu et al., 2015a). In addition, increased temperatures may also accelerate NH_3 volatilization from fertilizers, animal manure, or vehicles (Kang et al., 2016; Sutton et al., 2013; Zhang et al., 2010). NH_3 VCDs decreased sharply into autumn (Fig. 5), mainly owing to the decrease in agricultural emissions and the rapid drop in temperature. The annual growth rate in

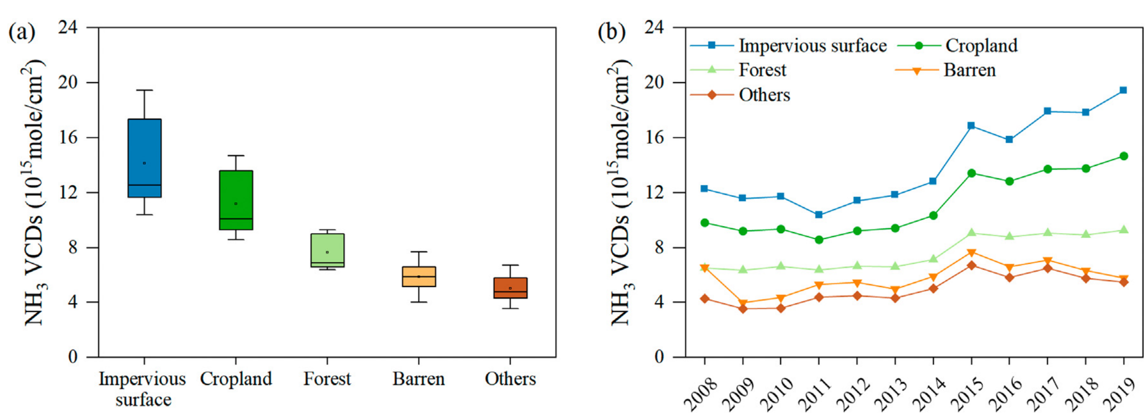

Fig. 4. Average NH_3 VCDs over different ground covers. (a) The average NH_3 VCDs over different land covers in China and (b) the interannual variation of the mean value of NH_3 VCDs over different land covers between 2008 and 2019.

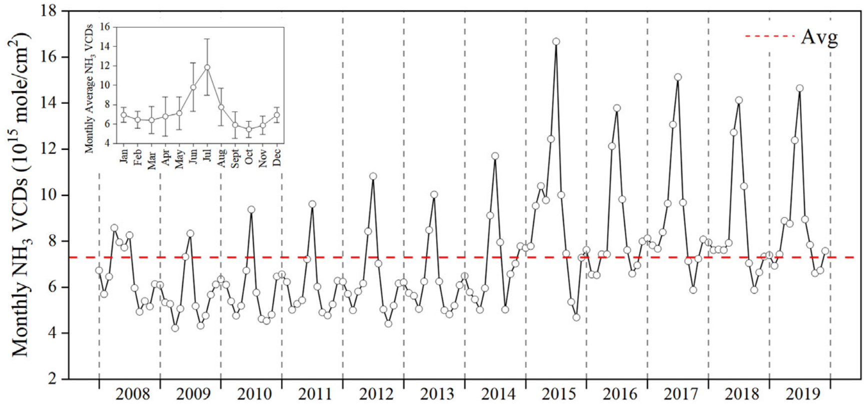

Fig. 5. Monthly trends of NH_3 VCDs in China monthly averages between 2008 and 2019.

summer was the highest (2.25 %) among the four seasons, with the most significant growth trend (tau = 0.70, $p < 0.01$) (Table S1).

3.2. Urban-rural variations

3.2.1. Urban-rural variations in temporal trends of NH_3 VCDs

In urban-rural analysis, urban areas were identified by urban extending products while non-urban areas were considered as rural areas. The average NH_3 VCDs in China's rural areas was 7.23×10^{15} molec·cm^{-2} from 2008 to 2019, with an annual growth rate of 2.48 % (Fig. 6). The average NH_3 VCDs in urban areas of China from 2008 to 2019 was 12.62×10^{15} molec·cm^2, 1.74 times higher than that in rural areas. The annual growth rate of NH_3 VCDs in urban areas was 3.98 %, which was 1.61 times higher than that in rural areas. This result is consistent with the ratio of mean values between urban and non-urban ground-based measurement sites nationwide (1.55) reported in other study (Pan et al., 2018b). We extracted ammonia concentration data from urban and rural sites with continuous observations in the Nationwide Nitrogen Deposition Monitoring Network (NNDMN) (Xu et al., 2015b) from 2012 to 2015, and calculated annual averages for urban and rural sites based on site type. The farmland sites have a high agricultural emission and thus have a high concentration of ammonia, which leads to a smaller urban-rural gap. We also found a similar temporal trend to this study (Fig. 6).

As previously mentioned, the high-density emissions from urban areas are the main reason for their high NH_3 VCDs. Urbanization also impacts the meteorological conditions and atmospheric environment of urban areas (Dai et al., 2019). With increased urbanization and climate warming, sources in cities will emit more NH_3 (Warner et al., 2017; Xu et al., 2020; Lan et al., 2021). With increased urbanization and climate warming, sources in cities will emit more NH_3 (Gu et al., 2022). Climate change is an important factor contributing to the future growth of NH_3 VCDs (Shen et al., 2020; Xu et al., 2021). Rural areas showed a slow interannual trend which may be owing to the reduction of emissions from agricultural sources as a result of scientific fertilizer structure, fertilizer application techniques, and farming techniques (Liao et al., 2022).

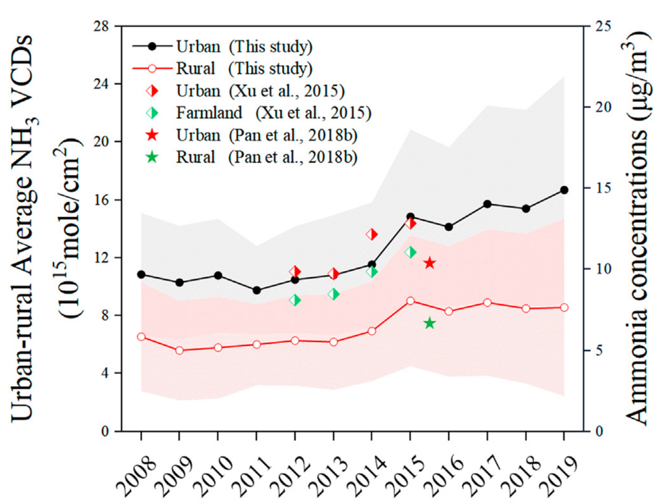

Fig. 6. Temporal trends in annual average NH3 VCDs and ground measured ammonia concentrations in urban and rural China.

3.2.2. Urban-rural gradient of NH_3 VCDs

From our analysis of the urban-rural gradient of NH_3 VCDs in provincial capital cities, we found that the average gradient showed a trend of gradually decreasing from urban to rural areas (Fig. 7a). The average urban-rural ratio of 31 cities is 1.11 which is similar to Xu et al. (2015b) study (the average ratio of urban to farmland is 1.19, range 1.15–1.23). The average trend in the provincial capital (D_{50}, the ratio of average NH_3 VCDs in the 50 km buffer zone around the urban area) was stable (Fig. 7a). In cold spot cities, NH_3 VCDs increased along the urban-rural gradient. In hotspot cities, NH_3 VCDs decreased along the urban-rural gradient (Fig. 7a). With increasing NH_3 VCDs in both urban and rural areas, the urban-rural ratio has not changed significantly (Fig. 7b). This indicates that the urban and rural NH_3 VCDs have the same growth trend. However, the urban-rural gap has shown a significant growth trend (Fig. S2).

Urbanization has significant impacts on the atmospheric environment and meteorological conditions (Dai et al., 2019). There were obvious variations in the urban-rural gradients of meteorological parameters between different cities (Fig. S3). Urban temperatures were generally higher than rural areas, with the maximum temperature difference between cold spot cities and hot spot cities being 0.15 K and 1.78 K, respectively, and hot spot cities being eleven times higher than cold spot cities. In cold spot cities, the wind speed was larger in urban areas and smaller in rural areas. In hot spot cities, the wind speed was small in urban areas but large in rural areas. In the cold spot cities, the urban-rural variations of precipitation were small. In hot spot cities, precipitation in urban areas was smaller than in rural areas. In urban areas, the high temperatures increase NH_3 emissions, decreased precipitation reduces NH_3 deposition, and reduced wind speed hinders the diffusion of NH_3. We found a significant correlation between the gradient of the 12-year average NH_3 VCDs in urban and rural areas and the gradient of the 12-year average meteorological parameters in 31 cities (Table S2). Lan et al. (2021) also indicated that meteorological parameters were closely related to the changes in NH_3 concentrations in both urban and rural areas.

3.3. Spatio-temporal characteristics of the influencing factors

In this study, we obtained the average contribution (Fig. 8a) and interannual trends of the factors influencing NH_3 VCDs (Fig. 8b) between 2008

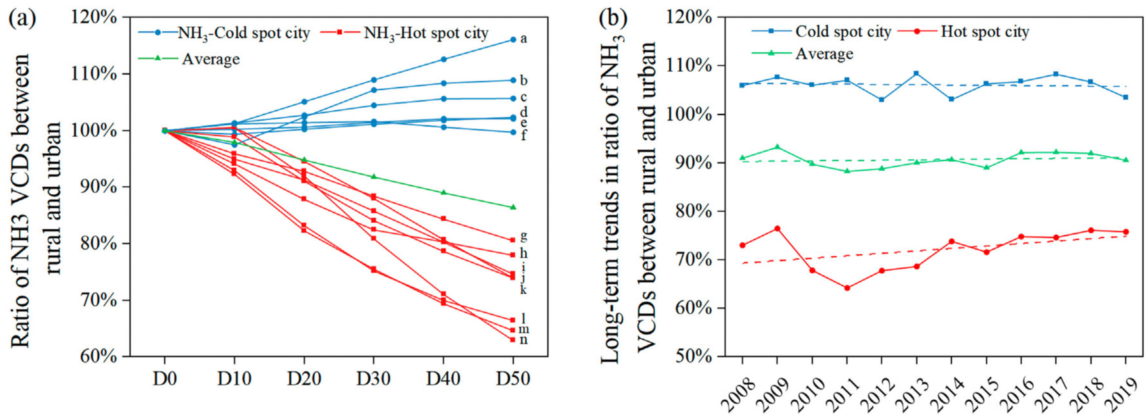

Fig. 7. Ratio of average NH_3 VCDs in buffer zones to urban areas. (a) The ratio of average NH_3 VCDs in the circular buffer zones of different distances to the urban area for each city (a. Jinan; b. Shanghai; c. Zhengzhou; d. Guiyang; e. Wuhan; f. Changsha; g. Taiyuan; h. Beijing; i. Xian; j. Shijiazhuang; k. Lanzhou; l. Huhehaote; m. Wulumuqi; n. Yinchuan). (b) Temporal trends of the ratio of annual average NH_3 VCDs in the 50 km buffer zones near the urban area to urban area from 2008 to 2019. (D_0, D_{10}, …, $D_{40,}$ and D_{50} represent the ratio of the average value of NH_3 VCDs in the 0 km, 10 km, …, 40 km, and 50 km circular buffer zone from the urban area to urban area, respectively).

and 2019 by the GTWR model. The R^2 of the predicted and actual values of GTWR is 0.90, which is significant. The contribution of meteorological parameters was the largest (averaged 30.13 %) and showed significant interannual fluctuations (ranged from 26.52 % to 35.29 %). The average contribution of social factors was 27.40 %. The annual average contribution of social factors showed an inverted U-shape, which was consistent with the "Kuznets curve". This might be result from the transformation of social development (Xu et al., 2020). The high contribution of social factors reflects the high correlation between ammonia concentration and intensive human activities and urbanization. The average contribution of atmospheric acidic gases was 23.20 %. Acidic gases have a negative effect on NH_3 VCDs, and the lower the concentration of acidic gases, the higher NH_3 VCDs. The contribution of acid gases has shown a remarkable increasing trend from 2012 (16.98 %) to 2018 (28.96 %), which was consistent with the trend of acid gas concentration (Liu et al., 2017a; Liu et al., 2019; Wang et al., 2017). The decrease in the concentration of atmospheric acid gases was the main cause of the increase in NH_3 VCDs (Liu et al., 2017a; Liu et al., 2019; Liu et al., 2017c). The average contribution of NH_3 emissions to NH_3 VCDs was 19.28 % and trended downward overall. This is because ammonia emissions directly affect NH_3 VCDs, and the emissions of NH_3 have gradually decreased in recent years (Liao et al., 2022).

The contribution of the factors has obvious spatial variations (Fig. 9). Region with the highest contribution of meteorological parameters was south China (averaged 38.33 %). Compared to the spatial distribution of the contribution of meteorological parameters in 2011 (Fig. 8a), the range of meteorological parameters was expanding in 2019. This may be influenced by the warming (Sutton et al., 2013). Region with the lowest contribution of acid gases was central China (averaged 14.50 %). The concentration of atmospheric acidic gases negatively correlated with the contribution rate (Liu et al., 2019). In general, ammonia was not sensitive to acid gases because the concentration of SO_2 was already low in north China, while NH_3 VCDs were relatively high (Xi et al., 2021; Xing et al., 2019; Ye et al., 2022). This may be the reason why the temporal variation in NH_3 VCDs lagged behind that in the atmospheric acidic gas concentration. Region with the highest contribution of NH_3 emissions was central China (averaged 28.20 %). This was consistent with the spatial distribution of ammonia emissions (Liao et al., 2022). Region with the highest contribution of social factors was north China (averaged 35.27 %). This indicates that the dominant ammonia concentration in north China was affected by intensive human activities and urbanization.

4. Conclusions

Currently, China is experiencing serious NH_3 pollution, so the spatial and temporal distributions of NH_3 in the country and the long-term trends of its influencing factors must be studied. However, few researchers have analyzed the factors influencing NH_3 from multiple perspectives. Most researchers have ignored both the factors influencing NH_3 on a national scale and the urban-rural variations in NH_3 concentrations. In this study, in conjunction with IASI-obtained NH_3 VCDs, we analyzed the temporal and spatial characteristics and long-term trends of NH_3 from 2008 to 2019. We analyzed the contributions of influencing factors (meteorological

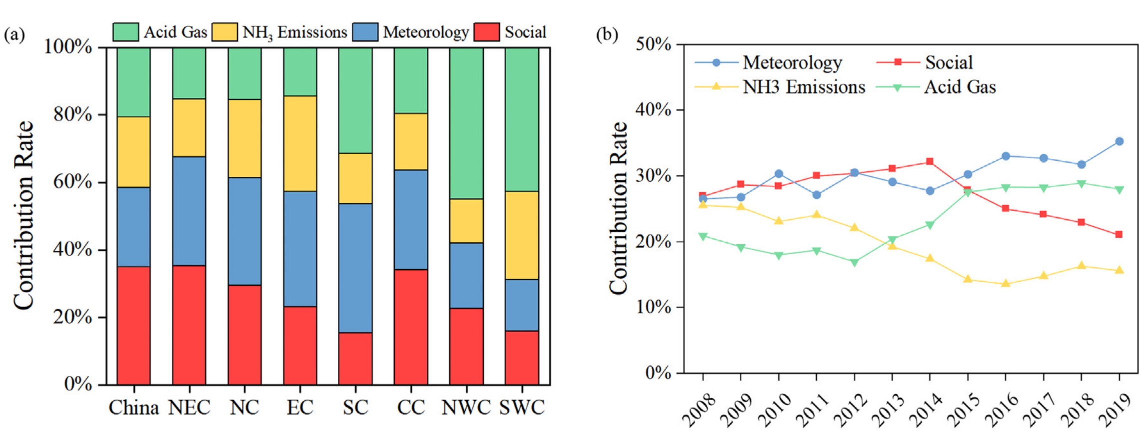

Fig. 8. Average contributions (a) and temporal trends (b) of the four influencing factors to NH_3 VCDs from 2008 to 2019. (a) Average contributions of influencing factors in different regions between 2008 and 2019. (b) Temporal trends in the annual contribution of impact factors between 2008 and 2019.

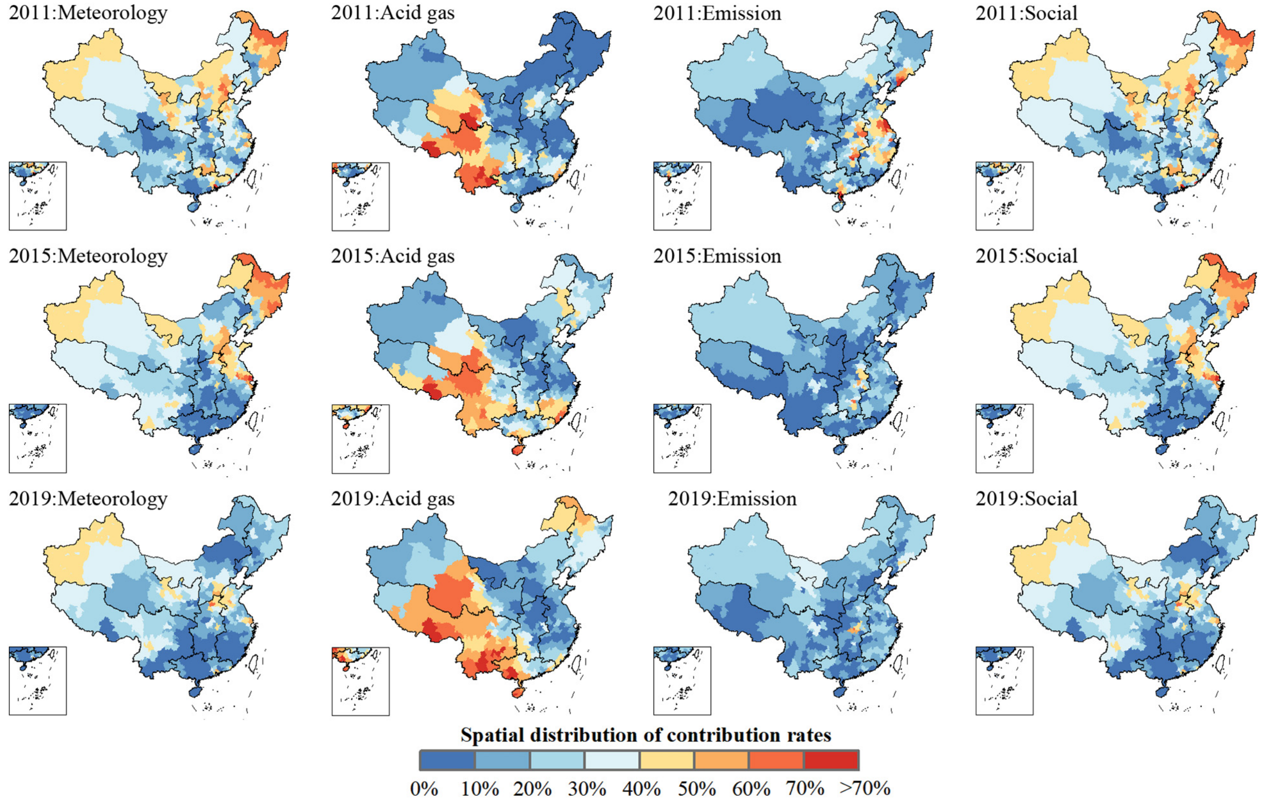

Fig. 9. Spatial distribution of the contribution of NH_3 VCDs impact factors.

parameters, atmospheric acid gas environment, emissions, and society) to NH_3 VCDs using the GTWR method.

The study showed that NH_3 VCDs have increased significantly during the period 2008–2019, with an increase of 31.88 %. There was a statistically significant aggregation in the distribution of NH_3 VCDs, and the high-value areas are mainly concentrated in the North China Plain and the Sichuan Basin. The highest NH_3 VCDs over impervious surfaces were mainly caused by urbanization. NH_3 VCDs increased rapidly in summer and declined quickly in NH_3 VCDs in autumn. This was due to seasonal variations in fertilization and meteorological conditions. A relatively unbalanced development between urban and rural areas in China caused the ratio between NH_3 VCDs in urban and rural areas to be relatively high (~1.74). The average annual growth rates of urban and rural NH_3 VCDs were 3.98 % and 2.48 %, respectively. In general, the urban-rural gradient of NH_3 VCDs showed a downward trend from urban to rural areas, and the urban-rural gap was expanding. The average contributions of meteorological parameters, social factors, atmospheric acid gas and NH_3 emission factors to NH_3 VCDs during the study period were 30.13 %, 27.40 %, 23.20 %, and 19.28 %, respectively, and showed substantial spatiotemporal heterogeneity. Reducing NH_3 concentrations is a complex issue that is influenced by various factors. For example, in recent years, NH_3 VCDs in NCP have been rapidly increasing. The response of acidic gases to NH_3 VCDs in NCP is gradually decreasing. The control of atmospheric particulate matter through the reduction of acid gases is limited. Therefore, we can consider the synergistic emission reduction of acid gases and ammonia in NCP.

This study still has some limitations. First, there may have some uncertainty in the processing of the satellite data. But we have performed quality control and compared it with the data obtained by error-weighted averaging with refined processing. Second, NH_3 VCDs was not verified temporally and spatially with ground measurements. Ground measurements have significant advantages in accuracy, and can effectively evaluate the accuracy and reliability of NH_3 concentration. We have also utilized ground measurements to compare urban-rural differences. Third, we only analyzed the urban-rural gradient in provincial capitals, but we believe that these cities are regionally representative. Fourth, due to data availability, we used NH_3 emissions data from 2017 instead of 2018. But we believed that one year of missing data wouldn't affect the overall trend. In addition, due to the limited IASI satellite observations, we did not conduct daily-scale analysis. Meanwhile, the influence of ammonia on secondary ammonium compounds was not evaluated in order to examine the impact of NH_3 consumption/emission.

We provide several suggestions for controlling atmospheric NH_3 in China. First, the financial support for NH_3 pollution control should be increased, considering that reducing ammonia is more cost-effective than reducing nitrogen oxides in mitigating air pollution (Gu et al., 2021). Second, the monitoring and control of urban emission sources should be strengthened to cope with the growth in NH_3 emissions in cities, such as phasing out high-emission vehicles and increasing the proportion of new-energy vehicles. Finally, control policies must fully consider the spatial and temporal trends in the influencing factors.

CRediT authorship contribution statement

Jinyan Dong: Conceptualization, Methodology, Software, Writing – original draft, Data curation. **Baojie Li:** Conceptualization, Writing – review & editing, Resources, Supervision. **Yan Li:** Resources. **Rui Zhou:** Investigation, Resources. **Cong Gan:** Resources. **Yongqi Zhao:** Resources. **Rui Liu:** Investigation. **Yating Yang:** Investigation. **Teng Wang:** Resources. **Hong Liao:** Supervision.

Data availability

Data will be made available on request.

Declaration of competing interest

The authors declare that they have no known competing financial interests or personal relationships that could have appeared to influence the work reported in this paper.

Acknowledgments

This research has been supported by the National Natural Science Foundation of China [Grant 42007381 and 42107385], the Natural Science Foundation of Jiangsu Province [Grant BK20200812, BK20220031 and BK20200515], and the National Key Research and Development Program of China [Grant 2020YFA0607803].

Appendix A. Supplementary data

Supplementary data to this article can be found online at https://doi.org/10.1016/j.scitotenv.2023.163733.

References

An, Z., Huang, R.-J., Zhang, R., Tie, X., Li, G., Cao, J., Zhou, W., Shi, Z., Han, Y., Gu, Z., Ji, Y., 2019. Severe haze in northern China: a synergy of anthropogenic emissions and atmospheric processes. Proc. Natl. Acad. Sci. U. S. A. 116, 8657–8666. https://doi.org/10.1073/pnas.1900125116.

Chen, S., Cheng, M., Guo, Z., Xu, W., Du, X., Li, Y., 2020. Enhanced atmospheric ammonia (NH3) pollution in China from 2008 to 2016: evidence from a combination of observations and emissions. Environ. Pollut. 263, 114421. https://doi.org/10.1016/j.envpol.2020.114421.

Chu, H.-J., Huang, B., Lin, C.-Y., 2015. Modeling the spatio-temporal heterogeneity in the PM10-PM2.5 relationship. Atmos. Environ. 102, 176–182. https://doi.org/10.1016/j.atmosenv.2014.11.062.

Clarisse, L., Clerbaux, C., Dentener, F., Hurtmans, D., Coheur, P.-F., 2009. Global ammonia distribution derived from infrared satellite observations. Nat.Geosci. 2, 479–483. https://doi.org/10.1038/ngeo551.

Dai, J., Wang, X., Dai, W., Chang, M., 2019. The impact of inhomogeneous urban canopy parameters on meteorological conditions and implication for air quality in the Pearl River Delta region. Urban Clim. 29, 100494. https://doi.org/10.1016/j.uclim.2019.100494.

Deng, Z., Zhang, Q., Zhang, X., 2021. Satellite-based analysis of spatial-temporal distributions of NH3 and factors of influence in North China. Front. Environ. Sci. 9, 761557. https://doi.org/10.3389/fenvs.2021.761557.

Fowler, D., Coyle, M., Skiba, U., Sutton, M.A., Cape, J.N., Reis, S., Sheppard, L.J., Jenkins, A., Grizzetti, B., Galloway, J.N., Vitousek, P., Leach, A., Bouwman, A.F., Butterbach-Bahl, K., Dentener, F., Stevenson, D., Amann, M., Voss, M., 2013. The global nitrogen cycle in the twenty-first century. Phil. Trans. R. Soc. B 368, 20130164. https://doi.org/10.1098/rstb.2013.0164.

Franco, B., Clarisse, L., Stavrakou, T., Müller, J.-F., Van Damme, M., Whitburn, S., Hadji-Lazaro, J., Hurtmans, D., Taraborrelli, D., Clerbaux, C., Coheur, P.-F., 2018. A general framework for global retrievals of trace gases from IASI: application to methanol, formic acid, and PAN. J. Geophys. Res. Atmos. 123. https://doi.org/10.1029/2018JD029633.

Fu, X., Wang, S.X., Ran, L.M., Pleim, J.E., Cooter, E., Bash, J.O., Benson, V., Hao, J.M., 2015. Estimating NH3 emissions from agricultural fertilizer application in China using the bi-directional CMAQ model coupled to an agro-ecosystem model. Atmos. Chem. Phys. 15, 6637–6649. https://doi.org/10.5194/acp-15-6637-2015.

Getis, A., Ord, J.K., 2010. The analysis of spatial association by use of distance statistics. Geogr. Anal. 24, 189–206. https://doi.org/10.1111/j.1538-4632.1992.tb00261.x.

Gong, P., Li, X., Zhang, W., 2019. 40-year (1978–2017) human settlement changes in China reflected by impervious surfaces from satellite remote sensing. Sci.Bull. 64, 756–763. https://doi.org/10.1016/j.scib.2019.04.024.

Gu, B., Zhang, L., Van Dingenen, R., Vieno, M., Van Grinsven, H.J., Zhang, X., Zhang, S., Chen, Y., Wang, S., Ren, C., Rao, S., Holland, M., Winiwarter, W., Chen, D., Xu, J., Sutton, M.A., 2021. Abating ammonia is more cost-effective than nitrogen oxides for mitigating PM2.5 air pollution. Science 374, 758–762. https://doi.org/10.1126/science.abf8623.

Gu, M., Pan, Y., Sun, Q., Walters, W.W., Song, L., Fang, Y., 2022. Is fertilization the dominant source of ammonia in the urban atmosphere? Sci. Total Environ. 838, 155890. https://doi.org/10.1016/j.scitotenv.2022.155890.

He, Y., Xu, R., Prior, S.A., Yang, D., Yang, A., Chen, J., 2021. Satellite-detected ammonia changes in the United States: natural or anthropogenic impacts. Sci. Total Environ. 789, 147899. https://doi.org/10.1016/j.scitotenv.2021.147899.

Hickman, J.E., Andela, N., Tsigaridis, K., Galy-Lacaux, C., Ossohou, M., Dammers, E., Van Damme, M., Clarisse, L., Bauer, S.E., 2021. Continental and ecoregion-specific drivers of atmospheric NO2 and NH3 seasonality over Africa revealed by satellite observations. Glob. Biogeochem. Cycles 35. https://doi.org/10.1029/2020GB006916.

Huang, B., Wu, B., Barry, M., 2010. Geographically and temporally weighted regression for modeling spatio-temporal variation in house prices. Int. J. Geogr. Inf. Sci. 24, 383–401. https://doi.org/10.1080/13658810802672469.

Kang, Y., Liu, M., Song, Y., Huang, X., Yao, H., Cai, X., Zhang, H., Kang, L., Liu, X., Yan, X., He, H., Zhang, Q., Shao, M., Zhu, T., 2016. High-resolution ammonia emissions inventories in China from 1980 to 2012. Atmos. Chem. Phys. 16, 2043–2058. https://doi.org/10.5194/acp-16-2043-2016.

Kendall, M.G., 1975. Rank Correlation Measures. Charles Griffin, London, p. 202.

Kuang, W., Chi, W., Lu, D., Dou, Y., 2014. A comparative analysis of megacity expansions in China and the U.S.: patterns, rates and driving forces. Landsc. Urban Plan. 132, 121–135. https://doi.org/10.1016/j.landurbplan.2014.08.015.

Lan, Z., Lin, W., Pu, W., Ma, Z., 2021. Measurement report: exploring NH3 behavior in urban and suburban Beijing: comparison and implications. Atmos. Chem. Phys. 21, 4561–4573. https://doi.org/10.5194/acp-21-4561-2021.

Li, M., Liu, H., Geng, G., Hong, C., Liu, F., Song, Y., Tong, D., Zheng, B., Cui, H., Man, H., Zhang, Q., He, K., 2017. Anthropogenic emission inventories in China: a review. Natl. Sci. Rev. 4, 834–866. https://doi.org/10.1093/nsr/nwx150.

Li, B., Chen, L., Shen, W., Jin, J., Wang, T., Wang, P., Yang, Y., Liao, H., 2021. Improved gridded ammonia emission inventory in China. Atmos. Chem. Phys. 21, 15883–15900. https://doi.org/10.5194/acp-21-15883-2021.

Liao, W., Liu, M., Huang, X., Wang, T., Xu, Z., Shang, F., Song, Y., Cai, X., Zhang, H., Kang, L., Zhu, T., 2022. Estimation for ammonia emissions at county level in China from 2013 to 2018. Sci. China Earth Sci. 65, 1116–1127. https://doi.org/10.1007/s11430-021-9897-3.

Liu, L., Zhang, X., Xu, W., Liu, X., Li, Y., Lu, X., Zhang, Y., Zhang, W., 2017a. Temporal characteristics of atmospheric ammonia and nitrogen dioxide over China based on emission data, satellite observations and atmospheric transport modeling since 1980. Atmos. Chem. Phys. 17, 9365–9378. https://doi.org/10.5194/acp-17-9365-2017.

Liu, L., Zhang, X., Xu, W., Liu, X., Lu, X., Wang, S., Zhang, W., Zhao, L., 2017b. Ground ammonia concentrations over China derived from satellite and atmospheric transport modeling. Remote Sens. 9, 467. https://doi.org/10.3390/rs9050467.

Liu, X., Xu, W., Duan, L., Du, E., Pan, Y., Lu, X., Zhang, L., Wu, Z., Wang, X., Zhang, Ying, Shen, J., Song, L., Feng, Z., Liu, Xueyan, Song, W., Tang, A., Zhang, Yangyang, Zhang, X., Collett, J.L., 2017c. Atmospheric nitrogen emission, deposition, and air quality impacts in China: an overview. Curr. Pollut.Rep. 3, 65–77. https://doi.org/10.1007/s40726-017-0053-9.

Liu, M., Huang, X., Song, Y., Xu, T., Wang, S., Wu, Z., Hu, M., Zhang, L., Zhang, Q., Pan, Y., Liu, X., Zhu, T., 2018. Rapid SO2 emission reductions significantly increase tropospheric ammonia concentrations over the North China Plain. Atmos. Chem. Phys. 18, 17933–17943. https://doi.org/10.5194/acp-18-17933-2018.

Liu, M., Huang, Xin, Song, Y., Tang, J., Cao, J., Zhang, X., Zhang, Q., Wang, S., Xu, T., Kang, L., Cai, X., Zhang, H., Yang, F., Wang, H., Yu, J.Z., Lau, A.K.H., He, L., Huang, Xiaofeng, Duan, L., Ding, A., Xue, L., Gao, J., Liu, B., Zhu, T., 2019. Ammonia emission control in China would mitigate haze pollution and nitrogen deposition, but worsen acid rain. Proc. Natl. Acad. Sci. U. S. A. 116, 7760–7765. https://doi.org/10.1073/pnas.1814880116.

Ma, S., 2020. High-resolution assessment of ammonia emissions in China: inventories, driving forces and mitigation. Atmos. Environ. 229, 117458. https://doi.org/10.1016/j.atmosenv.2020.117458.

Mann, H.B., 1945. Nonparametric tests against trend. Econometrica 13, 245. https://doi.org/10.2307/1907187.

Möller, D., Schieferdecker, H., 1985. A relationship between agricultural NH3 emissions and the atmospheric SO2 content over industrial areas. Atmos. Environ. 1967 (19), 695–700. https://doi.org/10.1016/0004-6981(85)90056-3.

Pan, Y., Tian, S., Liu, D., Fang, Y., Zhu, X., Zhang, Q., Zheng, B., Michalski, G., Wang, Y., 2016. Fossil fuel combustion-related emissions dominate atmospheric ammonia sources during severe haze episodes: evidence from 15 N-stable isotope in size-resolved aerosol ammonium. Environ. Sci. Technol. 50, 8049–8056. https://doi.org/10.1021/acs.est.6b00634.

Pan, Y., Tian, S., Liu, D., Fang, Y., Zhu, X., Gao, M., Wentworth, G.R., Michalski, G., Huang, X., Wang, Y., 2018a. Source apportionment of aerosol ammonium in an ammonia-rich atmosphere: an isotopic study of summer clean and hazy days in urban Beijing. J.Geophys.Res. Atmos. 123, 5681–5689. https://doi.org/10.1029/2017JD028095.

Pan, Y., Tian, S., Zhao, Y., Zhang, L., Zhu, X., Gao, J., Huang, W., Zhou, Y., Song, Y., Zhang, Q., Wang, Y., 2018b. Identifying ammonia hotspots in China using a National Observation Network. Environ. Sci. Technol. 52, 3926–3934. https://doi.org/10.1021/acs.est.7b05235.

Qiao, X., Ying, Q., Li, X., Zhang, H., Hu, J., Tang, Y., Chen, X., 2018. Source apportionment of PM2.5 for 25 Chinese provincial capitals and municipalities using a source-oriented community multiscale air quality model. Sci. Total Environ. 612, 462–471. https://doi.org/10.1016/j.scitotenv.2017.08.272.

Reche, C., Viana, M., Karanasiou, A., Cusack, M., Alastuey, A., Artiñano, B., Revuelta, M.A., López-Mahía, P., Blanco-Heras, G., Rodríguez, S., Sánchez de la Campa, A.M., Fernández-Camacho, R., González-Castanedo, Y., Mantilla, E., Tang, Y.S., Querol, X., 2015. Urban NH3 levels and sources in six major Spanish cities. Chemosphere 119, 769–777. https://doi.org/10.1016/j.chemosphere.2014.07.097.

Sampson, P.D., Richards, M., Szpiro, A.A., Bergen, S., Sheppard, L., Larson, T.V., Kaufman, J.D., 2013. A regionalized national universal kriging model using partial least squares regression for estimating annual PM2.5 concentrations in epidemiology. Atmos. Environ. 75, 383–392. https://doi.org/10.1016/j.atmosenv.2013.04.015.

Sharma, S.K., Kumar, M., Rohtash, Gupta, N.C., Saraswati, Saxena, M., Mandal, T.K., 2014. Characteristics of ambient ammonia over Delhi, India. Meteorol. Atmos. Phys. 124, 67–82. https://doi.org/10.1007/s00703-013-0299-8.

Shen, H., Chen, Y., Hu, Y., Ran, L., Lam, S.K., Pavur, G.K., Zhou, F., Pleim, J.E., Russell, A.G., 2020. Intense warming will significantly increase cropland ammonia volatilization threatening food security and ecosystem health. One Earth 3, 126–134. https://doi.org/10.1016/j.oneear.2020.06.015.

Shephard, M.W., Cady-Pereira, K.E., 2015. Cross-track Infrared Sounder (CrIS) satellite observations of tropospheric ammonia. Atmos. Meas. Tech. 8, 1323–1336. https://doi.org/10.5194/amt-8-1323-2015.

Streets, D.G., Bond, T.C., Carmichael, G.R., Fernandes, S.D., Fu, Q., He, D., Klimont, Z., Nelson, S.M., Tsai, N.Y., Wang, M.Q., Woo, J.-H., Yarber, K.F., 2003. An inventory of gaseous and primary aerosol emissions in Asia in the year 2000: AEROSOL EMISSION INVENTORY. J. Geophys. Res. 108. https://doi.org/10.1029/2002JD003093.

Sun, K., Tao, L., Miller, D.J., Pan, D., Golston, L.M., Zondlo, M.A., Griffin, R.J., Wallace, H.W., Leong, Y.J., Yang, M.M., Zhang, Y., Mauzerall, D.L., Zhu, T., 2017. Vehicle emissions as an important urban ammonia source in the United States and China. Environ. Sci. Technol. 51, 2472–2481. https://doi.org/10.1021/acs.est.6b02805.

Sutton, M.A., Reis, S., Riddick, S.N., Dragosits, U., Nemitz, E., Theobald, M.R., Tang, Y.S., Braban, C.F., Vieno, M., Dore, A.J., Mitchell, R.F., Wanless, S., Daunt, F., Fowler, D., Blackall, T.D., Milford, C., Flechard, C.R., Loubet, B., Massad, R., Cellier, P., Personne, E., Coheur, P.F., Clarisse, L., Van Damme, M., Ngadi, Y., Clerbaux, C., Skjøth, C.A., Geels, C., Hertel, O., Wichink Kruit, R.J., Pinder, R.W., Bash, J.O., Walker, J.T., Simpson, D., Horváth, L., Misselbrook, T.H., Bleeker, A., Dentener, F., de Vries, W., 2013. Towards a climate-dependent paradigm of ammonia emission and deposition. Phil. Trans. R. Soc. B 368, 20130166. https://doi.org/10.1098/rstb.2013.0166.

Van Damme, M., Clarisse, L., Heald, C.L., Hurtmans, D., Ngadi, Y., Clerbaux, C., Dolman, A.J., Erisman, J.W., Coheur, P.F., 2014. Global distributions, time series and error characterization of atmospheric ammonia (NH3) from IASI satellite observations. Atmos. Chem. Phys. 14, 2905–2922. https://doi.org/10.5194/acp-14-2905-2014.

Van Damme, M., Clarisse, L., Dammers, E., Liu, X., Nowak, J.B., Clerbaux, C., Flechard, C.R., Galy-Lacaux, C., Xu, W., Neuman, J.A., Tang, Y.S., Sutton, M.A., Erisman, J.W., Coheur, P.F., 2015. Towards validation of ammonia (NH3) measurements from the IASI satellite. Atmos. Meas. Tech. 8, 1575–1591. https://doi.org/10.5194/amt-8-1575-2015.

Van Damme, M., Whitburn, S., Clarisse, L., Clerbaux, C., Hurtmans, D., Coheur, P.-F., 2017. Version 2 of the IASI NH3 neural network retrieval algorithm: near-real-time and reanalysed datasets. Atmos. Meas. Tech. 10, 4905–4914. https://doi.org/10.5194/amt-10-4905-2017.

Wang, H., Wang, J., Huang, B., 2012. Prediction for spatio-temporal models with autoregression in errors. J.Nonparametr. Stat. 24, 217–244. https://doi.org/10.1080/10485252.2011.616893.

Wang, Y., Wang, H., Guo, H., Lyu, X., Cheng, H., Ling, Z., Louie, P.K.K., Simpson, I.J., Meinardi, S., Blake, D.R., 2017. Long-term O3–precursor relationships in Hong Kong: field observation and model simulation. Atmos. Chem. Phys. 17, 10919–10935. https://doi.org/10.5194/acp-17-10919-2017.

Warner, J.X., Wei, Z., Strow, L.L., Dickerson, R.R., Nowak, J.B., 2016. The global tropospheric ammonia distribution as seen in the 13-year AIRS measurement record. Atmos. Chem. Phys. 16, 5467–5479. https://doi.org/10.5194/acp-16-5467-2016.

Warner, J.X., Dickerson, R.R., Wei, Z., Strow, L.L., Wang, Y., Liang, Q., 2017. Increased atmospheric ammonia over the world's major agricultural areas detected from space: global atmospheric NH3 14 year trends. Geophys. Res. Lett. 44, 2875–2884. https://doi.org/10.1002/2016GL072305.

Whitburn, S., Van Damme, M., Clarisse, L., Bauduin, S., Heald, C.L., Hadji-Lazaro, J., Hurtmans, D., Zondlo, M.A., Clerbaux, C., Coheur, P.-F., 2016. A flexible and robust neural network IASI-NH3 retrieval algorithm. JGR Atmos. 121, 6581–6599. https://doi.org/10.1002/2016JD024828.

Wu, B., Li, R., Huang, B., 2014. A geographically and temporally weighted autoregressive model with application to housing prices. Int. J. Geogr. Inf. Sci. 28, 1186–1204. https://doi.org/10.1080/13658816.2013.878463.

Wu, S.-P., Dai, L.-H., Wei, Y., Zhu, H., Zhang, Y.-J., Schwab, J.J., Yuan, C.-S., 2018. Atmospheric ammonia measurements along the coastal lines of southeastern China: implications for inorganic nitrogen deposition to coastal waters. Atmos. Environ. 177, 1–11. https://doi.org/10.1016/j.atmosenv.2017.12.040.

Xi, Y., Zhu, J., Zhang, Q., Dai, G., He, N., Wang, Q., 2021. Hysteresis response of wet nitrate deposition to emission reduction in Chinese terrestrial ecosystems. Atmos. Environ. 260, 118555. https://doi.org/10.1016/j.atmosenv.2021.118555.

Xing, J., Zhang, F., Zhou, Y., Wang, S., Ding, D., Jang, C., Zhu, Y., Hao, J., 2019. Least-cost control strategy optimization for air quality attainment of Beijing–Tianjin–Hebei region in China. J. Environ. Manag. 245, 95–104. https://doi.org/10.1016/j.jenvman.2019.05.022.

Xu, W., Song, W., Zhang, Y., Liu, X., Zhang, L., Zhao, Y., Liu, D., Tang, A., Yang, D., Wang, D., Wen, Z., Pan, Y., Fowler, D., Collett Jr., J.L., Erisman, J.W., Goulding, K., Li, Y., Zhang, F., 2017. Air quality improvement in a megacity: implications from 2015 Beijing Parade Blue pollution control actions. Atmos. Chem. Phys. 17, 31–46. https://doi.org/10.5194/acp-17-31-2017.

Xu, W., Liu, L., Cheng, M., Zhao, Yuanhong, Zhang, L., Pan, Y., Zhang, Xiuming, Gu, B., Li, Y., Zhang, Xiuying, Shen, J., Lu, L., Luo, X., Zhao, Yu., Feng, Z., Collett Jr., J.L., Zhang, F., Liu, X., 2018. Spatial–temporal patterns of inorganic nitrogen air concentrations and deposition in eastern China. Atmos. Chem. Phys. 18, 10931–10954. https://doi.org/10.5194/acp-18-10931-2018.

Xu, W., Liu, X., Liu, L., Dore, A.J., Tang, A., Lu, L., Wu, Q., Zhang, Y., Hao, T., Pan, Y., Chen, J., Zhang, F., 2019a. Impact of emission controls on air quality in Beijing during APEC 2014: implications from water-soluble ions and carbonaceous aerosol in PM2.5 and their precursors. Atmos. Environ. 210, 241–252. https://doi.org/10.1016/j.atmosenv.2019.04.050.

Xu, W., Zhang, L., Liu, X., 2019b. A database of atmospheric nitrogen concentration and deposition from the nationwide monitoring network in China. Sci. Data 6, 51. https://doi.org/10.1038/s41597-019-0061-2.

Xu, P., Zhang, Y., Gong, W., Hou, X., Kroeze, C., Gao, W., Luan, S., 2015a. An inventory of the emission of ammonia from agricultural fertilizer application in China for 2010 and its high-resolution spatial distribution. Atmos. Environ. 115, 141–148. https://doi.org/10.1016/j.atmosenv.2015.05.020.

Xu, W., Luo, X.S., Pan, Y.P., Zhang, L., Tang, A.H., Shen, J.L., Zhang, Y., Li, K.H., Wu, Q.H., Yang, D.W., Zhang, Y.Y., Xue, J., Li, W.Q., Li, Q.Q., Tang, L., Lu, S.H., Liang, T., Tong, Y.A., Liu, P., Zhang, Q., Xiong, Z.Q., Shi, X.J., Wu, L.H., Shi, W.Q., Tian, K., Zhong, X.H., Shi, K., Tang, Q.Y., Zhang, L.J., Huang, J.L., He, C.E., Kuang, F.H., Zhu, B., Liu, H., Jin, X., Xin, Y.J., Shi, X.K., Du, E.Z., Dore, A.J., Tang, S., Collett, J.L., Goulding, K., Sun, Y.X., Ren, J., Zhang, F.S., Liu, X.J., 2015b. Quantifying atmospheric nitrogen deposition through a nationwide monitoring network across China. Atmos. Chem. Phys. 15, 12345–12360. https://doi.org/10.5194/acp-15-12345-2015.

Xu, P., Chen, A., Houlton, B.Z., Zeng, Z., Wei, S., Zhao, C., Lu, H., Liao, Y., Zheng, Z., Luan, S., Zheng, Y., 2020. Spatial variation of reactive nitrogen emissions from China's croplands codetermined by regional urbanization and its feedback to global climate change. Geophys. Res. Lett. 47. https://doi.org/10.1029/2019GL086551.

Xu, X., Ouyang, X., Gu, Y., Cheng, K., Smith, P., Sun, J., Li, Y., Pan, G., 2021. Climate change may interact with nitrogen fertilizer management leading to different ammonia loss in China's croplands. Glob. Chang. Biol. 27, 6525–6535. https://doi.org/10.1111/gcb.15874.

Yang, J., Huang, X., 2021. 30 m annual land cover and its dynamics in China from 1990 to 2019 (preprint). Data, Algorithms, And Models https://doi.org/10.5194/essd-2021-7.

Ye, Z., Li, J., Pan, Y., Wang, Z., Guo, X., Cheng, L., Tang, X., Zhu, J., Kong, L., Song, Y., Xing, J., Sun, Y., Pan, X., 2022. Synergistic effect of reductions in multiple gaseous precursors on secondary inorganic aerosols in winter under a meteorology-based redistributed daily NH3 emission inventory within the Beijing-Tianjin-Hebei region,China. Sci. Total Environ. 821, 153383. https://doi.org/10.1016/j.scitotenv.2022.153383.

Yu, F., Nair, A.A., Luo, G., 2018. Long-term trend of gaseous ammonia over the United States: modeling and comparison with observations. JGR Atmos. 123, 8315–8325. https://doi.org/10.1029/2018JD028412.

Zhang, Y., Dore, A.J., Ma, L., Liu, X.J., Ma, W.Q., Cape, J.N., Zhang, F.S., 2010. Agricultural ammonia emissions inventory and spatial distribution in the North China Plain. Environ. Pollut. 158, 490–501. https://doi.org/10.1016/j.envpol.2009.08.033.

Zhang, X., Wu, Y., Liu, X., Reis, S., Jin, J., Dragosits, U., Van Damme, M., Clarisse, L., Whitburn, S., Coheur, P.-F., Gu, B., 2017. Ammonia emissions may be substantially underestimated in China. Environ. Sci. Technol. 51, 12089–12096. https://doi.org/10.1021/acs.est.7b02171.

Zhang, Y., Benedict, K.B., Tang, A., Sun, Y., Fang, Y., Liu, X., 2020. Persistent nonagricultural and periodic agricultural emissions dominate sources of ammonia in urban Beijing: evidence from 15 N stable isotope in vertical profiles. Environ. Sci. Technol. 54, 102–109. https://doi.org/10.1021/acs.est.9b05741.

Zhao, M., Cheng, C., Zhou, Y., Li, X., Shen, S., Song, C., 2022. A global dataset of annual urban extents (1992–2020) from harmonized nighttime lights. Earth Syst. Sci. Data 14, 517–534. https://doi.org/10.5194/essd-14-517-2022.

Zheng, B., Tong, D., Li, M., Liu, F., Hong, C., Geng, G., Li, H., Li, X., Peng, L., Qi, J., Yan, L., Zhang, Y., Zhao, H., Zheng, Y., He, K., Zhang, Q., 2018. Trends in China's anthropogenic emissions since 2010 as the consequence of clean air actions. Atmos. Chem. Phys. 18, 14095–14111. https://doi.org/10.5194/acp-18-14095-2018.